NASA TECHNICAL NOTE

NASA TN D-6476

MIXING OF HYDROGEN INJECTED FROM MULTIPLE INJECTORS NORMAL TO A SUPERSONIC AIRSTREAM

by R. Clayton Rogers

Langley Research Center
Hampton, Va. 23365

NATIONAL AERONAUTICS AND SPACE ADMINISTRATION • WASHINGTON, D. C. • SEPTEMBER 1971

1. Report No. NASA TN D-6476	2. Government Accession No.
4. Title and Subtitle: MIXING OF HYDROGEN INJECTED FROM MULTIPLE INJECTORS NORMAL TO A SUPERSONIC AIRSTREAM	5. Report Date: September 1971
	6. Performing Organization Code
7. Author(s): R. Clayton Rogers	8. Performing Organization Report No. L-7896
	10. Work Unit No. 764-75-01-06
9. Performing Organization Name and Address: NASA Langley Research Center, Hampton, Va. 23365	11. Contract or Grant No.
	13. Type of Report and Period Covered: Technical Note
12. Sponsoring Agency Name and Address: National Aeronautics and Space Administration, Washington, D.C. 20546	14. Sponsoring Agency Code
15. Supplementary Notes	

16. Abstract

The mixing of hydrogen downstream of a row of sonic injectors normal to a Mach 4 airstream has been investigated to determine the effect of injector spacing. Injectors at spacing of 12.5 and 6.25 injector diameters were operated at ratios of jet dynamic pressure to free-stream dynamic pressure between 0.5 and 1.5. Nominal free-stream conditions were a stagnation temperature of 300 K and stagnation pressures of 1.38 and 2.07 MN/m^2. Turbulent-boundary-layer thickness at the injection station was 2.70 injector diameters. Measurements of hydrogen volume fraction and pitot and static pressures were made between 7 and 200 injector diameters downstream of the injectors. Results of the investigation indicated that the hydrogen penetration trajectory was not appreciably different from single-injector results, being proportional to the 0.300 power of the dynamic-pressure ratio. Maximum concentration decay with downstream distance for the wider injector spacing was correlated with the ratio of jet mass flux to free-stream mass flux; for the closer spacing, the rate of decay of the maximum concentration was inversely proportional to the 0.286 power of the ratio of jet mass flux to free-stream mass flux.

17. Key Words (Suggested by Author(s)): Injection; Jet mixing; Supersonic combustion	18. Distribution Statement: Unclassified – Unlimited

19. Security Classif. (of this report)	20. Security Classif. (of this page)	21. No. of Pages	22. Price*
Unclassified	Unclassified	34	$3.00

*For sale by the National Technical Information Service, Springfield, Virginia 22151

MIXING OF HYDROGEN INJECTED FROM MULTIPLE INJECTORS NORMAL TO A SUPERSONIC AIRSTREAM

By R. Clayton Rogers
Langley Research Center

SUMMARY

An investigation has been conducted to study the cold-flow mixing of hydrogen injected from multiple injectors oriented normal to a supersonic airstream. The injectors were flush mounted on a flat plate and laterally spaced at 12.5 and 6.25 injector diameters. Hydrogen was injected at sonic velocity and at ratios of jet dynamic pressure to free-stream dynamic pressure from 0.5 to 1.5 into a Mach 4.03 airstream having a stagnation temperature of 300 K and stagnation pressures of 13.6 and 20.4 atmospheres (1 atmosphere equals 101.3 kN/m^2). Corresponding Reynolds numbers per meter were 6.19×10^7 and 9.28×10^7, respectively, which gave a turbulent-boundary-layer thickness of 2.70 injector diameters at the injection station.

Measurements of hydrogen volume fraction and pitot and static pressures were made at 7, 30, 60, 120, and 200 injector diameters downstream of the injectors. The penetration of the hydrogen to the point at which the volume fraction was 0.005 was not appreciably different from single-injector data, being proportional to the 0.300 power of the dynamic-pressure ratio. Maximum concentration decay with downstream distance for the wider injector spacing was not significantly different from single injector data and was correlated with the mass-flux ratio. For the closer spacing, the rate of decay of maximum concentration was inversely proportional to the 0.286 power of the ratio of jet mass flux to free-stream mass flux. For both injector spacings, correlations were derived for the cold-flow mixing efficiency which related the fraction of injected hydrogen that could react to the initial jet and free-stream conditions and the injector size.

INTRODUCTION

The proposed use of a supersonic combustion ramjet as the propulsion system for advanced hypersonic aircraft during acceleration and cruise (for example, see ref. 1) requires an increased understanding of supersonic mixing and combustion processes. Design criteria for a supersonic combustor include the arrangement of fuel injectors to obtain the shortest mixing length and a uniform fuel distribution with minimum pressure losses. In-stream injection from a strut or other protrusion (refs. 2 to 5) may be

required for combustors with large internal dimensions. However, because existing scramjets are small scale, injection from the combustor wall has received serious and widespread attention. Some of the investigations of a wall-mounted injector injecting gas at sonic velocity and normal to a supersonic airstream are reported in references 6 to 14 for free-stream Mach numbers from 2.6 to 4.5 and ratios of jet dynamic pressure to free-stream dynamic pressure from 0.5 to 10. These data indicate jet penetrations less than 10 injector diameters which suggests that a combination of in-stream and wall injection would be necessary for some combustor designs.

Previous investigations (refs. 6 to 14) have considered only a single jet which permitted unrestrained lateral mixing, whereas a supersonic combustor would require multiple injectors. Single-jet data from reference 14 for sonic injection of hydrogen, at a ratio of jet dynamic pressure to free-stream dynamic pressure of 1.0 into a Mach 4 airstream with a turbulent-boundary-layer thickness of 2.70 injector diameters, showed that on the plate surface the jet spread laterally as much as 15 injector diameters on either side of the injector. It appears that constraining the lateral spreading of the jet by the addition of injectors to either side of the single jet would alter the downstream mixing. Data from reference 15 for multiple injectors at a spacing of 6.25 injector diameters and operating at a dynamic-pressure ratio of 1.0 substantiate this effect when compared with single-jet data from reference 14.

The present investigation was conducted to provide information on the penetration and mixing of hydrogen injected at sonic velocity from multiple, circular injectors laterally spaced in a line perpendicular to the airstream. The injectors had an exit diameter of 0.102 cm and were flush mounted perpendicular to the surface of a flat plate that spanned the 23-cm-square tunnel test section. The tests were conducted for injector spacings of 6.25 and 12.5 injector diameters at a free-stream Mach number of 4.03, stagnation temperature of 300 K, and stagnation pressures of 13.6 and 20.4 atmospheres (1 atmosphere equals 101.3 kN/m^2); corresponding Reynolds numbers per meter were 6.19×10^7 and 9.28×10^7, respectively. Boundary-layer thickness on the plate at the injection station was 2.7 injection diameters. Hydrogen was injected at sonic velocity over a range of pressures to obtain ratios of jet dynamic pressure to free-stream dynamic pressure from 0.5 to 1.5. Measurements of hydrogen volume fraction, pitot pressure, and static pressure were made by vertical and horizontal surveys of the flow field at 7, 30, 60, 120, and 200 injector diameters downstream of the injection station.

SYMBOLS

A stream-tube cross-sectional area, $meters^2$

d injector exit diameter, meters

d_j	effective jet exit diameter, $dK^{1/2}$, meters
$\bar{f}$	average hydrogen-air mass ratio
K	injector discharge coefficient
M	Mach number
$\dot{m}$	mass flow rate, kilograms/second
$\dot{m}_r$	ratio of integrated mass flow rate to measured injected mass flow rate, defined by equation (4)
p_t	absolute total pressure, newtons/meter^2 or atmospheres
q_r	ratio of jet dynamic pressure to free-stream dynamic pressure, $(\rho V^2)_j / (\rho V^2)_\infty$
s	injector or jet spacing, meters
V	velocity, meters/second
x	longitudinal coordinate
y	lateral coordinate
z	vertical coordinate
z'	nondimensional vertical coordinate (see eq. (3))
α	hydrogen mass fraction
β	air mass flux, $(\rho V)_x(1 - \alpha)$, kilograms/meter^2-second
λ	ratio of jet mass flux to free-stream mass flux, $(\rho V)_j / (\rho V)_\infty$
δ	boundary-layer thickness at injector station, meters
η_d	distortion efficiency defined by equation (2)

η_m mixing efficiency

ν hydrogen volume fraction

ξ hydrogen mass flux parameter, $\alpha(\rho V)_x/(\rho V)_j$

ρ mass density, kilograms/meter^3

Subscripts:

j jet conditions

max maximum

min minimum

o conditions at edge of mixing region where $\nu = 0.005$

x survey point or local conditions in mixing region

α conditions at which mass concentration is maximum

1 conditions in undisturbed flow upstream of injectors

5 location where mass concentration is half maximum

∞ free stream

APPARATUS AND PROCEDURE

Test Facility and Model

Five 0.102-cm-diameter sonic injectors with a lateral spacing parallel to the plate leading edge of 0.635 cm were flush mounted perpendicular to the plate surface 18.6 cm from the leading edge of the rectangular flat plate sketched in figure 1. The leading edge was a wedge on the bottom surface cut at 10^o with a tip hand sharpened to approximately 2^o; the resulting cylindrical leading edge was approximately 0.013 cm thick. The plate spanned the 23-cm-square test section of a continuous-flow Mach 4 wind tunnel. Nominal free-stream test conditions were a stagnation temperature of 300 K and stagnation pressures of 13.6 and 20.4 atmospheres (1 atmosphere equals 101.3 kN/m^2); corresponding

Reynolds numbers per meter were 6.19×10^7 and 9.28×10^7, respectively. A survey of the boundary layer on the flat plate at the injection station at these conditions (ref. 14) indicated a turbulent boundary layer 2.7 injector diameters thick. The Mach number above the boundary layer at the injector station was 4.03.

Injector Flow

A schematic of the hydrogen gas supply and sampling system is presented in figure 2. Each of the five injectors was supplied hydrogen by a 0.476-cm-diameter tube from the manifold. All the tubes except the center one were valved to permit selection of either a 0.635-cm or 1.270-cm (6.25 or 12.5 injector diameter) injector spacing. The hydrogen-jet stagnation temperature was measured with a standard iron-constantan thermocouple inserted in the manifold and had a nominal value of 300 K. Jet total pressure was measured by a wall static-pressure orifice mounted near the exit of the 0.476-cm-diameter supply tube for the center injector and was estimated to be within 99 percent of the true jet total pressure. The apparatus was operated over a jet total-pressure range from 2 to 4 atmospheres corresponding to ratios of jet dynamic pressure to free-stream dynamic pressure q_r of 0.5 to 1.5. Test conditions for a single injector are given in the following table:

q_r	$p_{t,\infty}$, atm	$p_{t,j}$, atm	$\dot{m}_j$, g/sec
0.5	20.4	1.986	0.0820
.75	20.4	2.980	.1230
1.0	13.6	2.647	.1094
1.5	13.6	3.960	.1641

Instrumentation

Gas analyzer.- During a survey, the volumetric concentration of hydrogen in the gas samples taken through the pitot probe was measured by a process gas chromatograph. (See refs. 16 and 17.) Full-scale chromatographic readings were obtained by drawing 100-percent-hydrogen samples from the supply manifold. Repeatability of the chromatographic readings checked to an accuracy of ±0.5 percent full scale which corresponds to an error of ±0.005 in the volume fraction or $\pm 3.5 \times 10^{-4}$ in the mass fraction. Cycle time of the chromatograph was 1 min and nitrogen was used as the carrier gas. Additional information about the chromatograph operation for these tests may be found in reference 14.

Probe description.- The gas-sampling pitot probe and static-pressure probe are shown in figure 3. The gas-sampling pitot probe was a boundary-layer survey type with the probe tip mounted in a 7.94-mm-diameter supporting tube offset to allow for actuator

rod clearance. The static-pressure probe was of similar design with a cone angle of 28° and four 0.203-mm-diameter orifices located 14 probe diameters from the tip. The actuator mechanism provided for probe movement for vertical traversing and yaw in the horizontal plane. Probe position accuracy of the actuator mechanism was ±0.127 mm (±0.125 injector diameter) for the vertical surveys and $\pm 0.10^{\circ}$ for the horizontal surveys over a yaw angle range of 10°.

Flow measurement.- The mass flow rate of the injected gas was measured with a 0.318-cm-diameter, sharp-edge, corner-tap orifice meter. The static temperature at the meter was assumed to be the same as the jet stagnation temperature. Injector discharge coefficients, based on orifice meter measurements, normally were between 0.73 and 0.78. Sample flow rate to the chromatograph and the bypassed flow rate were measured by thermoconductivity mass flowmeters. All pressures except the tunnel-wall static pressures were measured with strain-gage-type transducers and recorded by using automatic-balance potentiometers. The tunnel-wall static pressures were measured by mercury manometers and recorded periodically during each test.

Survey Procedure

One vertical and three horizontal surveys of the flow field were made at 7, 30, 60, 120, and 200 injector diameters downstream of the injectors. The vertical surveys were made along the center line of the center jet stepwise from the plate surface outward until a zero hydrogen concentration was obtained. Horizontal surveys were then made by yawing the probe at points above the plate corresponding to maximum and half-maximum concentrations and at a point midway between the plate surface and the point of maximum concentration. At each point in the surveys, a gas sample and a pitot-pressure measurement were taken. Only the data downstream of the center injector are presented herein even though each horizontal survey spanned the entire five-jet mixing region. These data are considered good for yaw angles less than 15°.

RESULTS AND DISCUSSION

Flow-Field Structure

Details of the flow-field structure in the vicinity of a single sonic injector have been studied in other investigations (for example, refs. 7, 8, 9, and 12) by using schlieren photographs. These data, which were generally for injection at values of q_r greater than 1.0 and into a boundary layer less than 1 injector diameter thick, indicated a separated boundary layer and a strong bow shock in the free stream. For a boundary layer approximately 3 injector diameters thick and a value of q_r near unity, references 13 and 14 show that the bow shock in the free stream is weaker and the separation is less extensive than for the thinner boundary layer. The general flow-field structure resulting

from multiple jets is presented in figure 4 and is very similar to that of the single jet of reference 14. The shape and location of the jet bow shock in the free stream were only slightly affected by q_r or jet spacing s/d. Figure 4 also presents typical profile data of hydrogen mass fraction behind the center injector at three downstream locations and concentration trajectories (lines tracing constant values of hydrogen concentration) for s/d of 6.25 and q_r of 1.0.

Penetration trajectories.- The penetration of a single sonic jet injected normal to a supersonic free stream has been discussed considerably in the literature. Although different definitions have been used, the term "penetration," denoted by $(z/d)_o$, is herein defined as the vertical height from the plate to the edge of the mixing region where the hydrogen volume fraction ν is one-half of 1 percent. The penetration trajectory is then defined as the variation with downstream distance of the jet penetration in the vertical center-line plane. Jet penetration is usually correlated as a function of jet and free-stream Mach numbers, dynamic-pressure ratio, and downstream distance. Figure 5 presents the trajectories of maximum concentration α_{max}, half-maximum concentration α_5, and jet penetration correlated with q_r for s/d of 12.5 and 6.25 and q_r from 0.5 to 1.5. Data from reference 14 for a single jet (s/d = ∞) at q_r of 1.0 is represented by the solid symbols for the α_{max} and α_5 trajectories. The penetration trajectories for the multiple jets are compared with the single-jet correlation from reference 14 for x/d less than 120 and q_r between 0.5 and 1.5. The correlation is expressed as

$$\left(\frac{z}{d}\right)_o = 3.87(q_r)^{0.300}\left(\frac{x}{d}\right)^{0.143} \tag{1}$$

Within the accuracy of the data points, estimated to be approximately 3 percent, the effect of spacing on the jet penetration trajectories is small. In figure 5(a) for s/d of 12.5, the multiple-jet half-maximum and maximum concentration trajectories do not increase as rapidly as those for the single jet. In figure 5(b) for s/d of 6.25, the effects of lateral interjet mixing on the maximum and half-maximum concentration trajectories become noticeable at x/d of about 60; the distance from the plate surface to α_{max} is nearly constant and the α_5 trajectories are independent of q_r.

Decay of maximum concentration.- The decay of maximum concentration with downstream distance for s/d of 12.5 and q_r between 0.5 and 1.5 is presented in figure 6(a) along with single-jet data from reference 14. The present data are not considerably different from the single-injector data; this suggests that for s/d of 12.5, the downstream mixing of the center injector is not appreciably influenced by adjacent injectors. The rate of decay of α_{max} is essentially constant for all test values of q_r. In figure 6(b), the maximum concentration is correlated with the ratio of jet mass flux to free-stream

mass flux. The slope of the correlating line is -0.69. The dynamic-pressure ratio is related to the mass-flux ratio by the factor of the ratio of jet-exit velocity to free-stream velocity, which had a constant value of 1.74.

Figure 7 presents the decay of maximum concentration with downstream distance for s/d of 6.25 along with the single-jet data of reference 14. In figure 7(a), a change in the value of q_r produces a corresponding change in the rate of decay of α_{max}, with the lowest value of q_r giving the fastest decrease in α_{max}. The slower decay of α_{max} for s/d of 6.25 as compared with the decay of α_{max} for s/d of 12.5 (fig. 6(a)) results from the lateral restriction imposed by adjacent jets on air entering the mixing region from each side. It can be seen from physical considerations of the $s/d = 6.25$ flow field that an increase in penetration produces a proportionate increase in air mass flow entering the mixing region; thus, the amount of air that mixes with the hydrogen from one jet increases as the 0.300 power of q_r (see eq. (1)). For constant free-stream conditions the mass flow rate of injected hydrogen increases directly with q_r. Thus, the overall hydrogen-air ratio in the mixing region of the center jet increases as the 0.7 power of q_r and the rate of mixing is retarded as q_r is increased. In figure 7(b), the decay of the maximum concentration is correlated with the 0.286 power of the mass-flux ratio. The slope of the correlating line is -0.333.

Lateral uniformity.- In the design of a supersonic combustor it is desirable to obtain a relatively uniform mixture. For these multiple injector tests, a measure of the uniformity of the mixing region was obtained by calculating the distortion factor presented in figure 8. The distortion factor is defined as the difference between the maximum and minimum mass fractions in the horizontal survey through the point of maximum concentration divided by α_{max}. For the configuration with wider spacing (fig. 8(a)), the high values of the distortion factor result from the small amount of merging between the flow fields of adjacent injectors. With the closer injector spacing (fig. 8(b)), the value of the distortion factor decreases rapidly with x/d downstream of $x/d = 60$. The distortion efficiency, defined as the value of the mean mass fraction in the horizontal survey through the point of maximum concentration as a fraction of α_{max}, is determined from

$$\eta_d = 1 - \frac{1}{2}\left(1 - \frac{\alpha_{min}}{\alpha_{max}}\right) \tag{2}$$

A reasonable value of the distortion factor is 0.20 which corresponds to a value of η_d of 0.90. Mixing lengths to obtain an η_d of 0.90 are given in figure 8 and are represented in figure 7(a) by the dash line which crosses the stoichiometric concentration (0.0285) at a value of q_r slightly greater than 0.5 and x/d of about 130.

Profile Data

Typical nondimensional profiles of hydrogen mass fraction obtained from the vertical surveys downstream of the center jet are presented in figure 9 for $s/d = 12.5$ and 6.25 and $q_r = 0.5$, 1.0, and 1.5. The origin of the vertical coordinate was shifted to the point at which maximum concentration occurred. The positive vertical coordinate is nondimensionalized by the difference between the location of half-maximum concentration and maximum concentration. Below the origin, the vertical coordinate is nondimensionalized by $(z/d)_{\alpha}$. At all downstream stations the data profiles above the point of maximum concentration are approximated by a Gaussian distribution of the following form:

$$\frac{\alpha}{\alpha_{max}} = \exp\left(-0.6935(z')^2\right) \tag{3}$$

where

$$z' = \begin{cases} \dfrac{z - z_{\alpha}}{z_5 - z_{\alpha}} & \left(z > z_{\alpha}\right) \\ \dfrac{z - z_{\alpha}}{z_{\alpha}} & \left(z < z_{\alpha}\right) \end{cases}$$

Below the point of α_{max} there is some scatter of the data, particularly for $s/d = 12.5$ and upstream of $x/d = 60$, but the Gaussian function gives a good average trend.

Typical nondimensional velocity profiles obtained from vertical surveys are presented in figure 10 for $s/d = 12.5$ and 6.25 and $q_r = 1.0$. The data are compared with data from reference 14 for the boundary-layer velocity profile at the injection station with no injection. The symbol V_o is defined as the velocity at the edge of the mixing region at a distance $(z/d)_o$ above the plate. There appears to be a peak in the velocity profiles, which generally corresponds to the point of maximum concentration and decreases with downstream distance as the profile shape approaches that of the boundary layer.

Typical nondimensional total-pressure profiles in the vertical plane are presented in figure 11 for $q_r = 1.0$ and $s/d = 12.5$ and 6.25. Also included from reference 14 is the boundary-layer total-pressure profile with no injection at the injection station. The profiles for both injector spacings are very similar, particularly in the extensive region of low total pressure. This low total-pressure region extends over approximately 60 percent of the height of the mixing region with total pressures less than 10 percent of free-stream pressure; the profiles are not significantly different from those of the single jet in reference 14. Nondimensional total-pressure distributions in the horizontal plane through the point of maximum concentration are presented in figure 12. The lateral

coordinate is nondimensionalized by the injector spacing. At x/d greater than 30, the data for the wider spacing show total pressures of less than 10 percent of free-stream pressure extending over 35 percent of the width of the mixing region with maximum total pressures in the region between adjacent injectors of about 25 percent of free stream. For $s/d = 6.25$, the total pressures are less than 6 percent of free-stream pressure over the entire width of the mixing region of the center jet. These low pressures are partly a result of the $s/d = 6.25$ maximum concentrations being closer to the plate surface as indicated in figure 5. The fraction of injected hydrogen contained within the region where the total pressure is less than 10 percent of free-stream pressure ranges from 0.90 to 0.76 for $s/d = 6.25$ and from 0.88 to 0.65 for $s/d = 12.5$ at x/d between 30 and 200. This result suggests that there is a large total-pressure loss associated with turning and accelerating the hydrogen jets. The total-pressure recoveries, based on the mass averaged total pressure in the undisturbed stream tube ahead of the injectors which contains the same mass flow of air as the center jet mixing region, are approximately 0.70 and 0.50 for $s/d = 12.5$ and $s/d = 6.25$, respectively. Data for a single injector (ref. 14) give a mass averaged total-pressure recovery of approximately 0.80.

Flow-Field Contours

Comparison of the integrated hydrogen mass flow rate, obtained from the normalized contours of the hydrogen mass flux parameter ξ, with metered flow rates of injected hydrogen provides an indication of the overall accuracy of the profile data. In terms of ξ, the ratio of contour-integrated mass flow rate to injected mass flow rate is

$$\dot{m}_r = \frac{4\xi_{max}A_o}{\pi d_j^2}\int_0^{1.0}\frac{\xi}{\xi_{max}}\,d\left(\frac{A}{A_o}\right) \tag{4}$$

where A_o is the area bounded by the zero concentration contour. Values of $\dot{m}_r$ from equation (4) are presented as a function of x/d in figure 13. The solid line is a straight-line least-squares fit to the average deviation of the points. The general trend of the data is to approach unity as x/d increases and q_r decreases. The large inaccuracies in $\dot{m}_r$ near the injectors result from the large negative gradient in the plate static pressure which extends to about 30 injector diameters downstream of the center injector (ref. 15) and from the associated large gradients in concentration and velocity near the injectors. For flow fields of this nature, however, differences of 20 percent between integrated and measured mass flow rates are considered typical.

Representative contours of hydrogen mass fraction in the YZ-plane at $x/d = 120$ and $q_r = 1.0$ are presented in figure 14. The dash lines in figures 14(b) and (c) are positioned at $\pm y/d$ equal to one-half the injector spacing and represent the dividing lines between adjacent injectors. Comparison of these contours with those for a single jet

($s/d = \infty$) from reference 14 (fig. 14(a)) indicates no appreciable difference for α greater than 0.01.

Typical contours of nondimensional air mass flux contained within the zero concentration contour at $x/d = 120$ and $q_r = 1.0$ are presented in figure 15. The similarity of the contours for $s/d = 12.5$ (fig. 15(b)) and those for a single jet (fig. 15(a)) is apparent. The contours for $s/d = 6.25$ are relatively flat (fig. 15(c)), as were the concentration contours (fig. 14(c)); this indicates that the flow field is becoming two-dimensional. The air mass flow rate within the mixing region of the center jet was obtained by evaluating the following integral:

$$\dot{m}_1 = \beta_{max} A_o \int_0^{1.0} \frac{\beta}{\beta_{max}} d\left(\frac{A}{A_o}\right) \tag{5}$$

Results of the integrations were used to determine the average hydrogen-air mass ratio based on the injected hydrogen mass flow rate and are compared in figure 16 with results for a single jet. At a given station, values of $\bar{f}$ for $s/d = 12.5$ are as much as 50 percent less than those for $s/d = 6.25$.

Mixing Efficiency

At any downstream station, a mixing efficiency η_m was defined as the fraction of the injected hydrogen that would react if complete chemical reaction occurred without further mixing. In the regions of the flow field where a lean hydrogen-air mixture exists, all the hydrogen was assumed to react; where a rich hydrogen-air mixture exists, the reactable hydrogen was considered that required to react with all the available oxygen. The mixing efficiency was obtained from contour integration of the center injector mixing region and is presented in figure 17 as a function of x/d and q_r for $s/d = 12.5$ and 6.25. Estimated accuracy of the values of mixing efficiency is 15 percent. The following correlations were derived for each injector spacing:

$$\eta_m = 0.485\left(\frac{x}{d} q_r^{-0.671}\right)^{0.149} \qquad \left(\frac{s}{d} = 12.5\right) \tag{6}$$

$$\eta_m = 0.297\left(\frac{x}{d} q_r^{-1.51}\right)^{0.210} \qquad \left(\frac{s}{d} = 6.25\right) \tag{7}$$

These correlations are considered applicable over a range of dynamic-pressure ratios from 0.5 to 1.5 for cold-flow mixing of hydrogen injected at sonic velocity and normal to a Mach 4 airstream with a zero pressure gradient except that caused by the injection disturbance. Thus, the rate of mixing is related to the jet and free-stream initial

conditions and the size and spacing of the injectors. At every downstream station, a higher value of η_m was obtained for the wider injector spacing and lower q_r. Calculations using single-jet data from reference 14 indicated a mixing efficiency only slightly less than that given by equation (6). Note that by definition of the mixing efficiency, the downstream station where η_m is first equal to 1 is also the point at which the maximum concentration has decayed to stoichiometric (figs. 7 and 8).

CONCLUDING REMARKS

An investigation to study the nonreactive mixing of hydrogen gas injected normal to a Mach 4.03 airstream from multiple sonic injectors laterally spaced at 12.5 and 6.25 injector diameters has been conducted for ratios of jet dynamic pressure to free-stream dynamic pressure q_r from 0.5 to 1.5. Surveys of the flow field were made at several stations downstream of the injector to obtain distributions of hydrogen concentration and pitot and static pressures. Examination of the results of the investigation indicated that the penetration trajectories for multiple jets are almost the same as those previously obtained for a single jet and correlate as a function of the 0.300 power of q_r. The maximum concentration trajectories (lines tracing constant values of hydrogen concentration) for the 6.25 injector diameter spacing s/d at stations x/d downstream of 60 injector diameters were essentially independent of q_r.

The decay of the maximum concentration for s/d of 12.5 was not significantly different from single-injector data and was inversely proportional to the 0.69 power of downstream distance. The rate of decay of the maximum concentration for s/d of 6.25 was a function of the mass-flux ratio λ; decay of the maximum concentration was correlated with the 0.286 power of λ and was inversely proportional to the 0.333 power of downstream distance.

The shape of nondimensional concentration profiles in the vertical center-line plane was independent of q_r and s/d and could be approximated by a Gaussian distribution at all downstream stations.

Total-pressure recoveries at downstream stations between 30 and 200 injector diameters were referred to the mass averaged total pressure in the undisturbed stream tube that was fueled by the hydrogen from the center injector and had average values of approximately 0.70 and 0.50 for $s/d = 12.5$ and 6.25, respectively.

A mixing efficiency parameter was defined as the fraction of injected hydrogen that would react if complete chemical reaction occurred without further mixing; this parameter was correlated with q_r and x/d for $s/d = 12.5$ and 6.25. At every downstream station, a higher mixing efficiency was obtained with the wider injector spacing; however,

the average hydrogen-air mass ratio for $s/d = 12.5$ was as much as 50 percent less than that for $s/d = 6.25$.

Langley Research Center,
National Aeronautics and Space Administration,
Hampton, Va., August 10, 1971.

REFERENCES

1. Henry, John R.; and McLellan, Charles H.: The Air-Breathing Launch Vehicle for Earth-Orbit Shuttle – New Technology and Development Approach. AIAA Paper No. 70-269, Feb. 1970.

2. Faucher, Joseph E., Jr.; Goldstein, Sidney; and Taback, Edward: Supersonic Combustion of Fuels Other Than Hydrogen for Scramjet Applications. AFAPL-TR-67-12, U.S. Air Force, Feb. 1967.

3. Povinelli, Louis A.; Povinelli, Frederick P.; and Hersch, Martin: A Study of Helium Penetration and Spreading in a Mach 2 Airstream Using a Delta Wing Injector. NASA TN D-5322, 1969.

4. Hersch, Martin; and Povinelli, Louis A.: Effect of Interacting Vortices on Jet Penetration Into a Supersonic Stream. NASA TM X-2134, 1970.

5. Becker, John V.: New Approaches to Hypersonic Aircraft. Paper presented at the Seventh Congress of the International Council of the Aeronautical Sciences (Rome, Italy), Sept. 14-18, 1970.

6. Vranos, Alexander; and Nolan, James J.: Supersonic Mixing of Helium and Air. Bumblebee Rep. No. TG 63-53, Appl. Phys. Lab., Johns Hopkins Univ., June 1964, pp. 131-161.

7. Spaid, F. W.; Zukoski, E. E.; and Rosen, R.: A Study of Secondary Injection of Gases Into a Supersonic Flow. Tech. Rep. No. 32-834, Jet Propulsion Lab., California Inst. Technol., Aug. 1, 1966.

8. Torrence, Marvin G.: Concentration Measurements of an Injected Gas in a Supersonic Stream. NASA TN D-3860, 1967.

9. Orth, R. C.; Schetz, J. A.; and Billig, F. S.: The Interaction and Penetration of Gaseous Jets in Supersonic Flow. NASA CR-1386, 1969.

10. Koch, Larry N.; and Collins, Daniel J.: The Effect of Varying Secondary Mach Number and Injection Angle on Secondary Gaseous Injection Into a Supersonic Flow. AIAA Paper No. 70-552, May 1970.

11. Chrans, Larry J.; and Collins, Daniel J.: Stagnation Temperature and Molecular Weight Effects in Jet Interaction. AIAA J., vol. 8, no. 2, Feb. 1970, pp. 287-293.

12. Cohen, Leonard S.; Coulter, Lawrence J.; and Chiappetta, Louis: Hydrocarbon-Fueled Scramjet. Vol. VII – Fuel Distribution Investigation. AFAPL-TR-68-146, Vol. VII, U.S. Air Force, Apr. 1970.

13. Torrence, Marvin G.: Effect of Injectant Molecular Weight on Mixing of a Normal Jet in a Mach 4 Airstream. NASA TN D-6061, 1971.

14. Rogers, R. Clayton: A Study of the Mixing of Hydrogen Injected Normal to a Supersonic Airstream. NASA TN D-6114, 1971.

15. McClinton, Charles Richard: The Effect of Injection Angle on the Interaction Between Sonic Secondary Jets and a Supersonic Freestream. M.S. Thesis, George Washington Univ., Feb. 1971.

16. Jeffery, P. G.; and Kipping, P. J.: Gas Analysis by Gas Chromatography. Macmillan Co., 1964.

17. Tranchant, Jean, ed.: Practical Manual of Gas Chromatography. Elsevier Pub. Co., 1969.

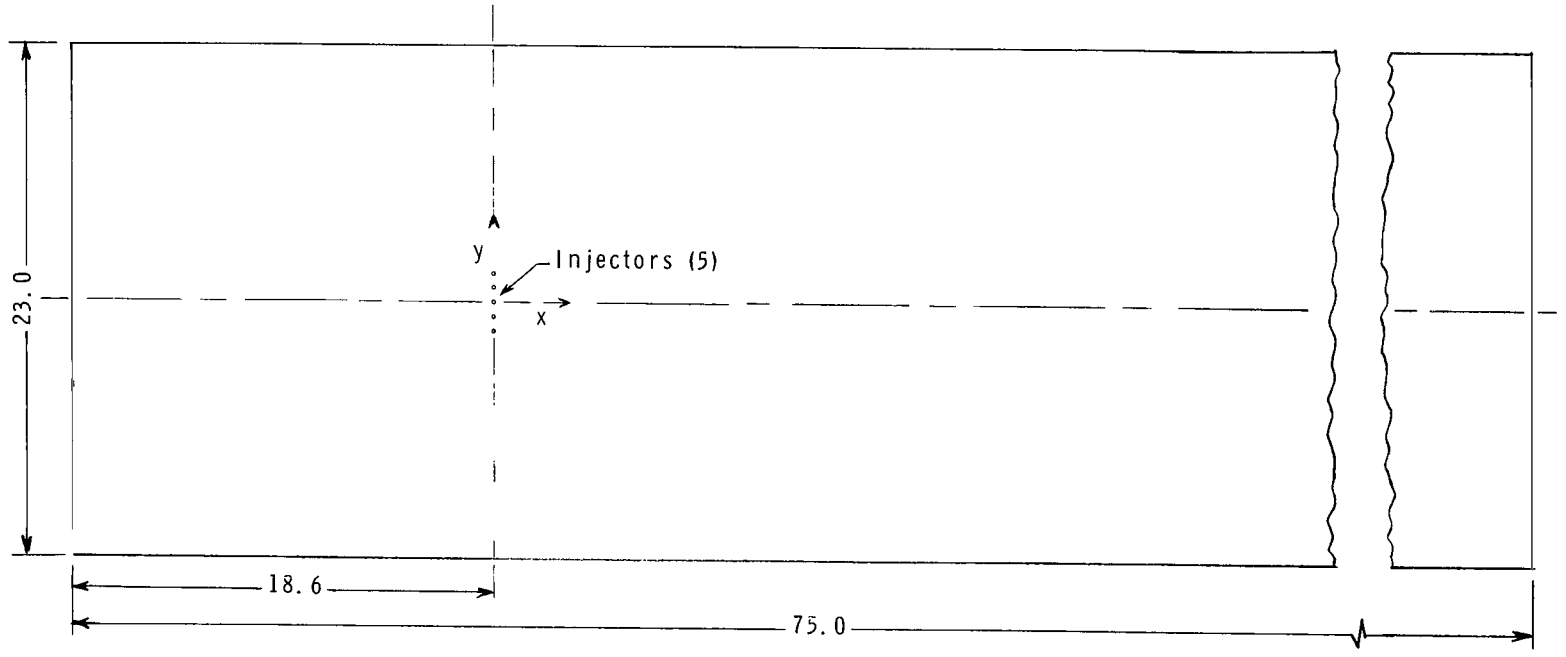

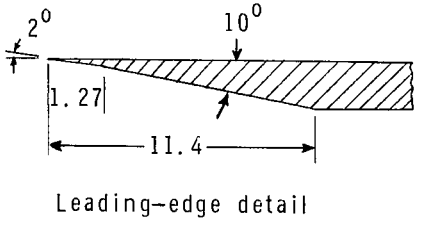

Leading-edge detail

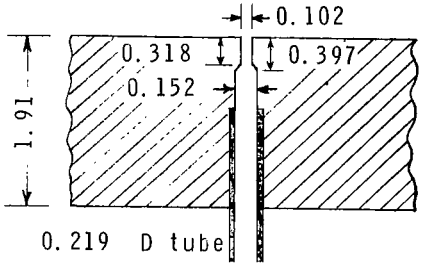

Nozzle detail

Figure 1.- Model details. All dimensions are in centimeters.

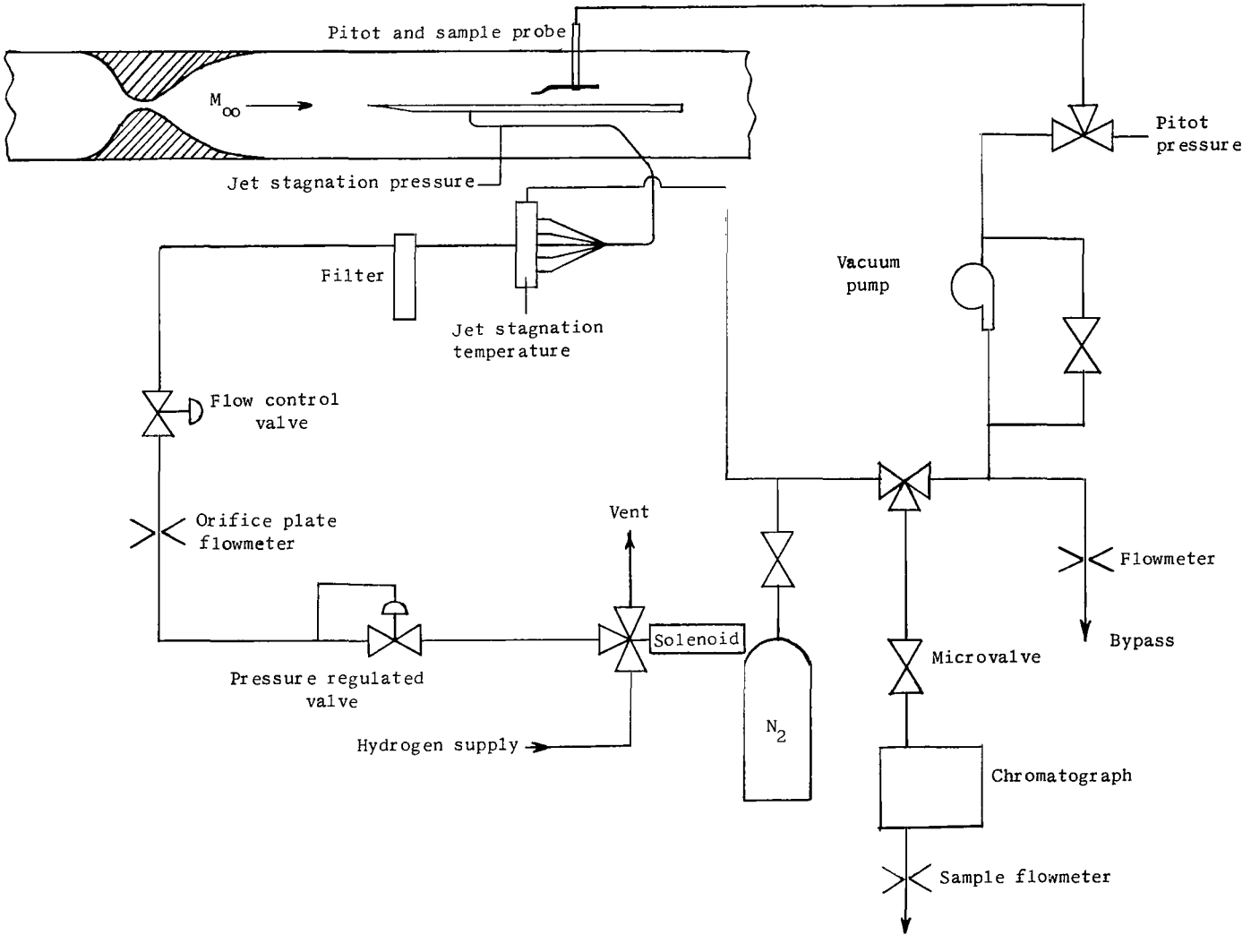

Figure 2.- Schematic of hydrogen gas supply and sampling system.

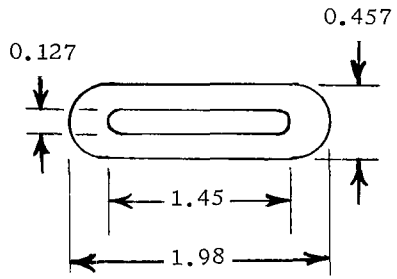

Probe tip

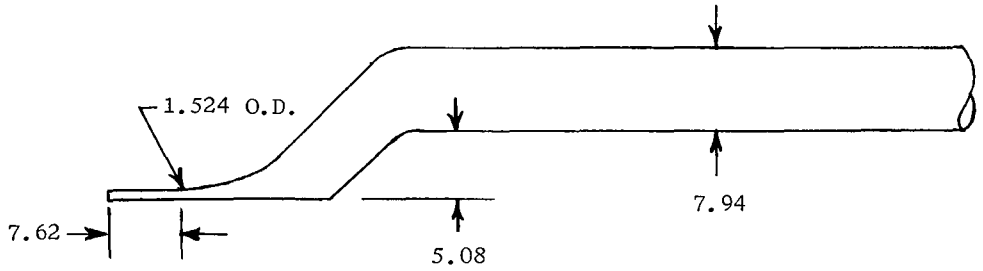

Gas-sampling probe

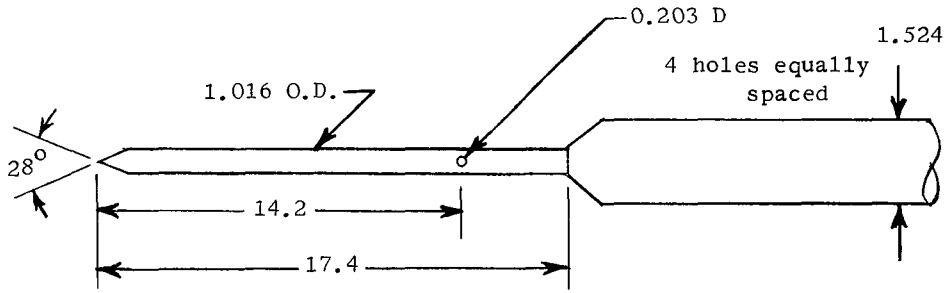

Static-pressure probe

Figure 3.- Survey-probe design. All dimensions are in millimeters.

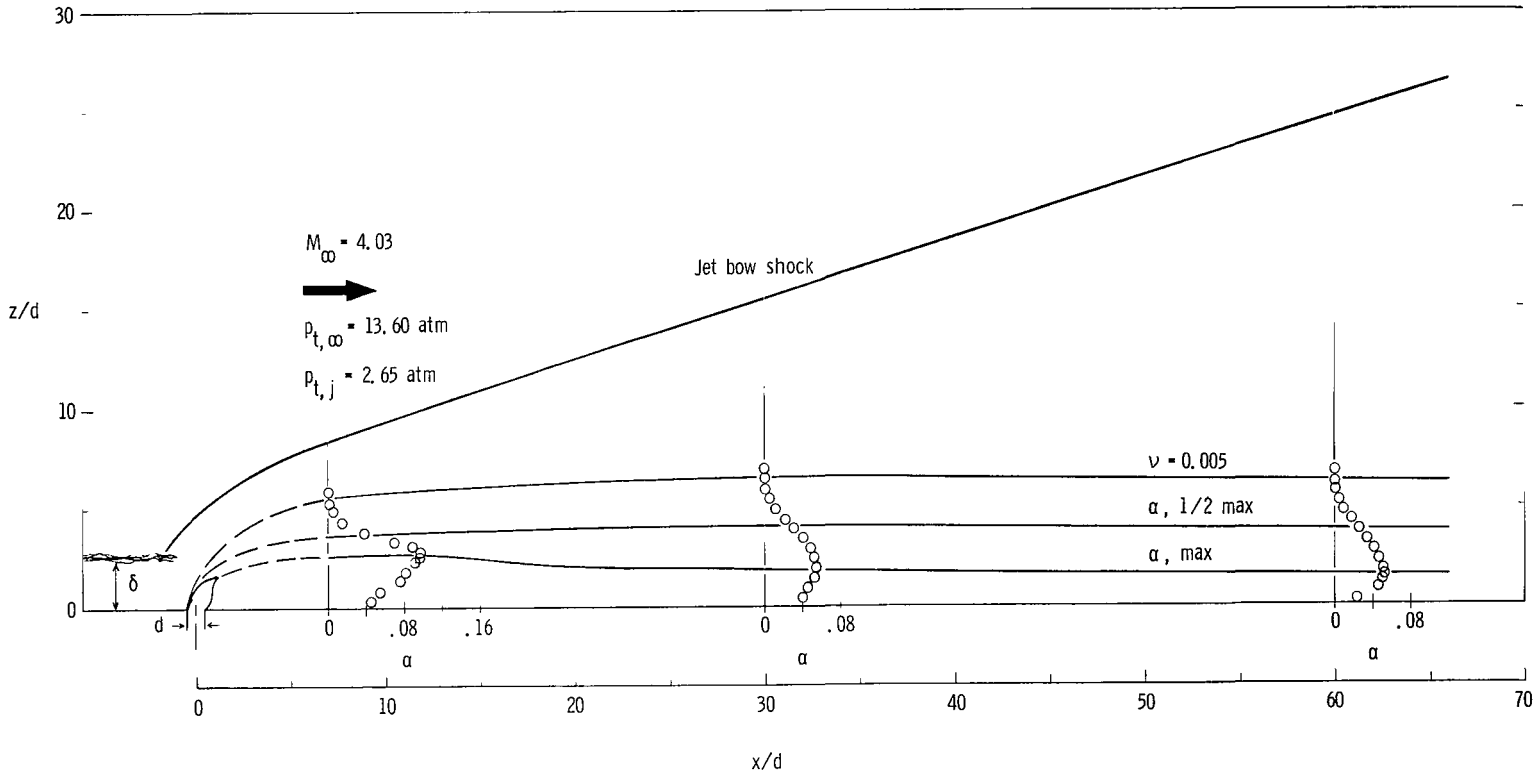

Figure 4.- Structure of flow field and mixing region. s/d = 6.25; q_r = 1.0.

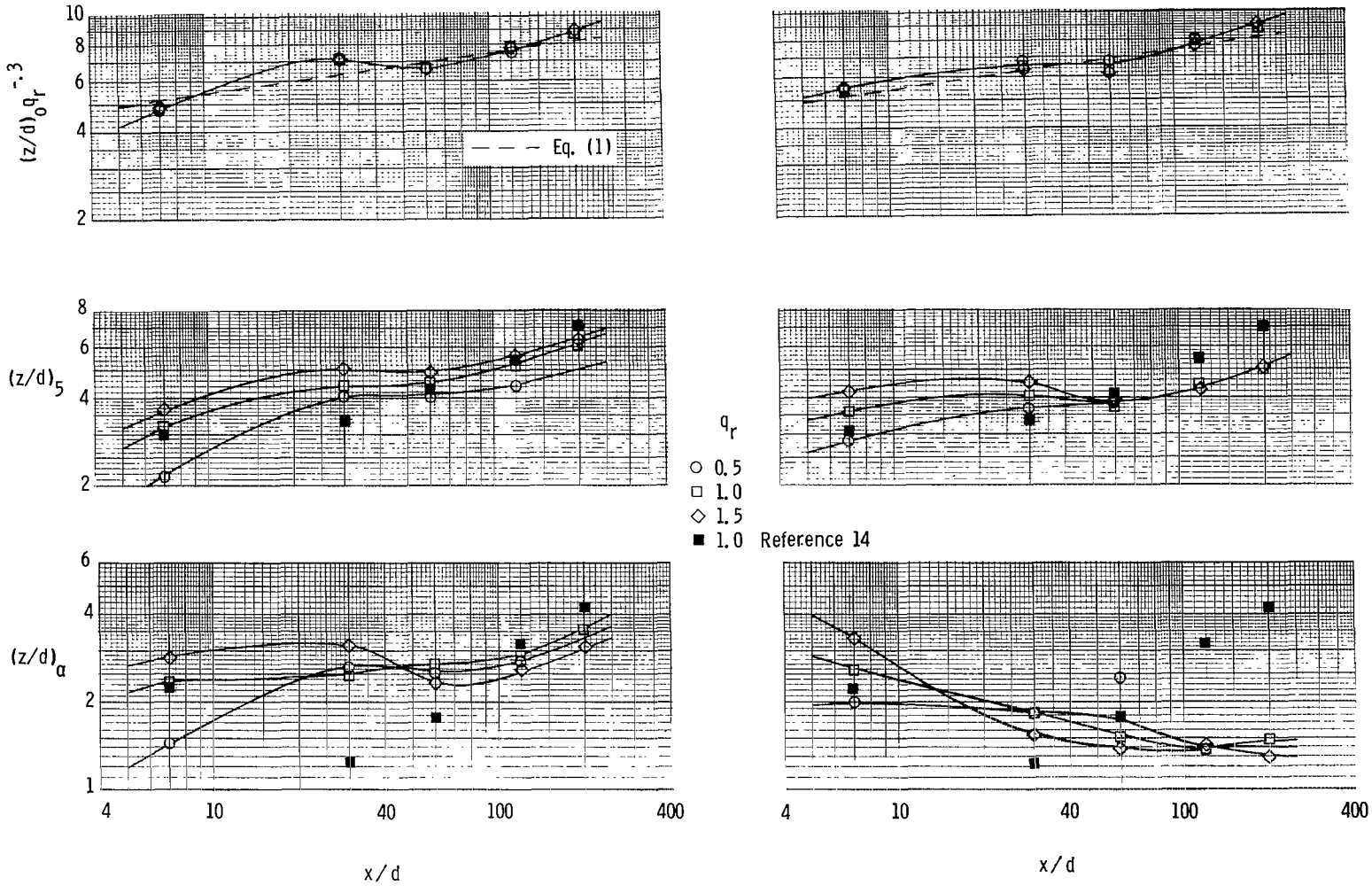

(a) s/d = 12.5.

(b) s/d = 6.25.

Figure 5.- Maximum concentration, half-maximum concentration, and jet penetration trajectories.

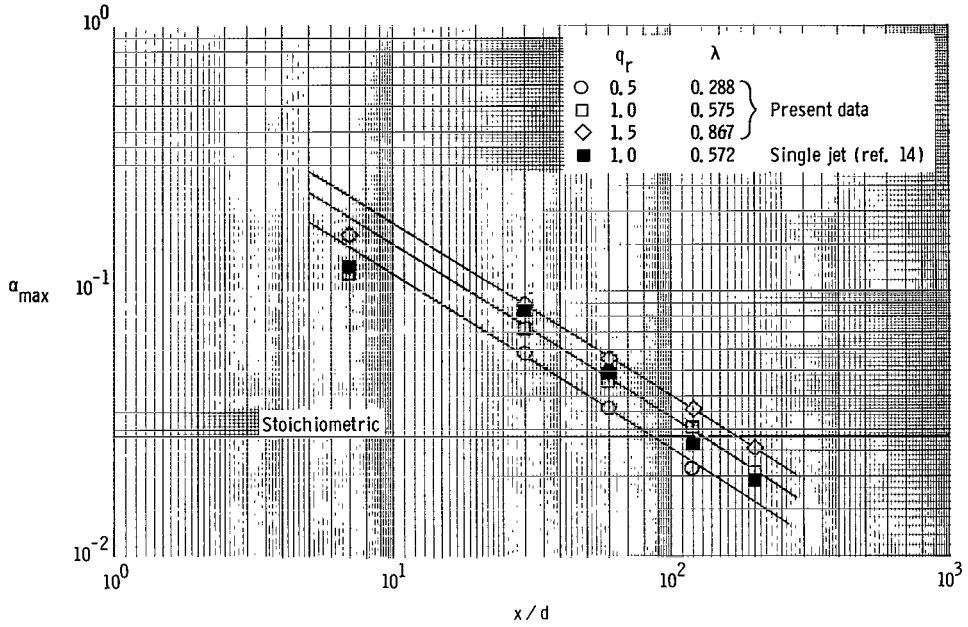

(a) Effect of dynamic-pressure ratio.

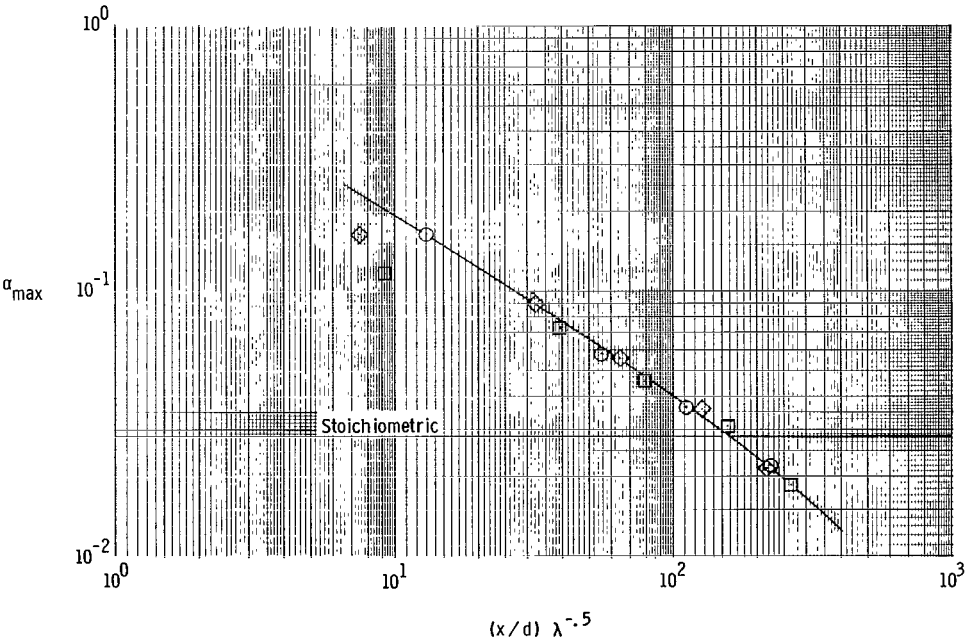

(b) Correlated with mass-flux ratio.

Figure 6.- Decay of maximum concentration with downstream distance. s/d = 12.5.

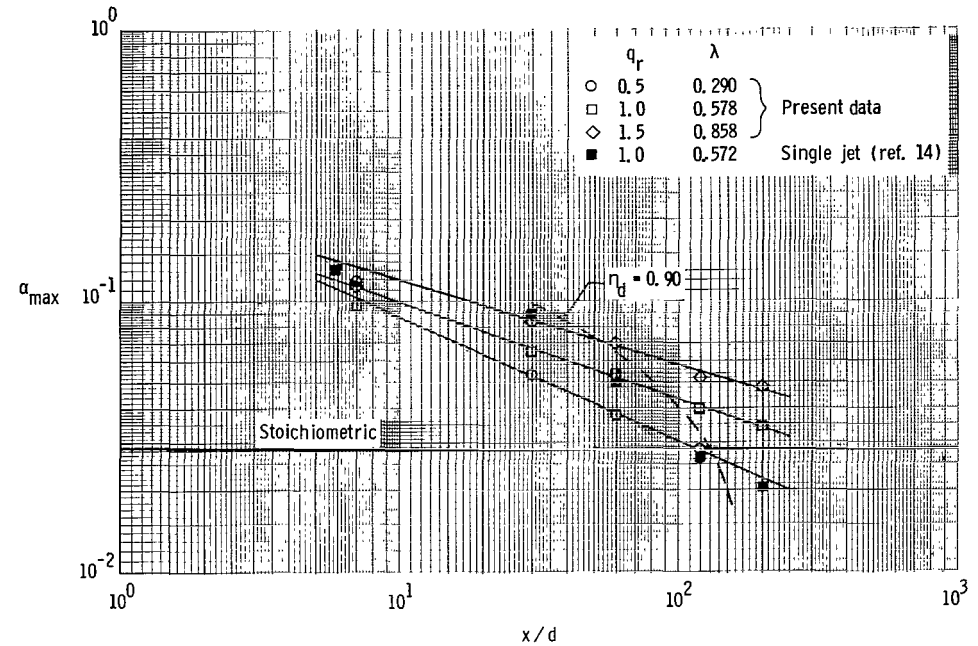

(a) Effect of dynamic-pressure ratio.

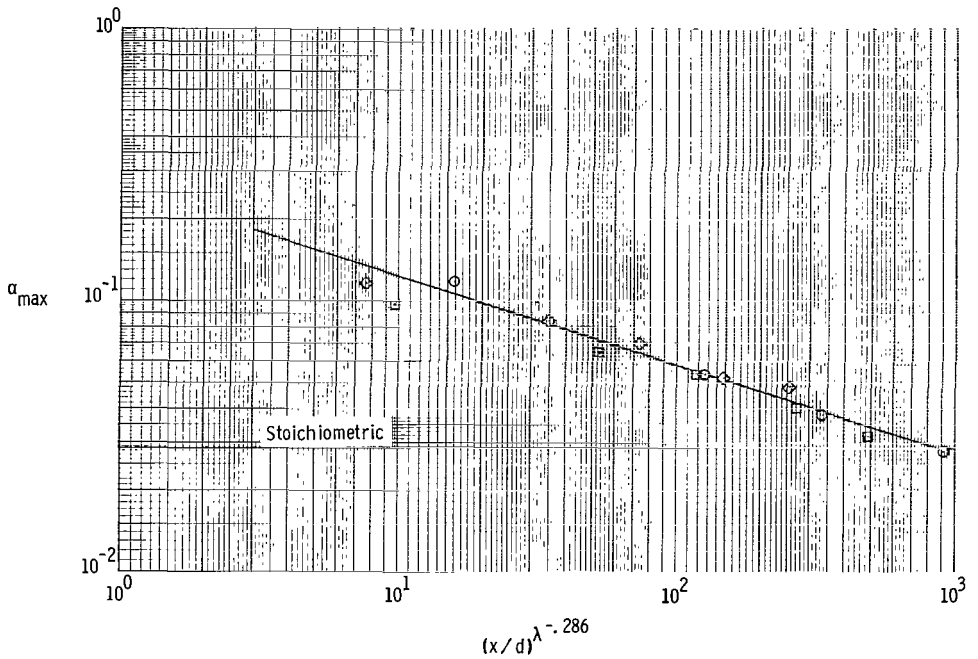

(b) Correlated with mass-flux ratio.

Figure 7.- Decay of maximum concentration with downstream distance. s/d = 6.25.

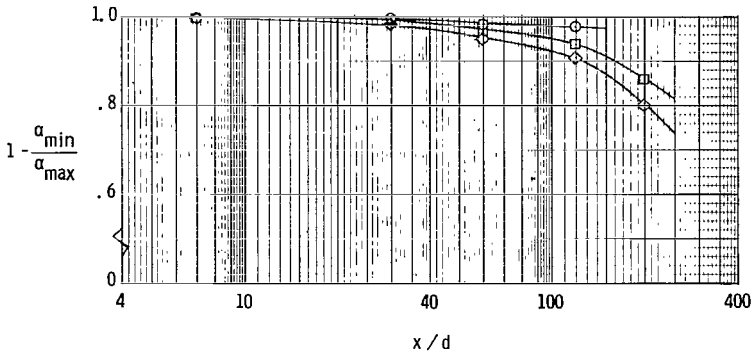

(a) s/d = 12.5.

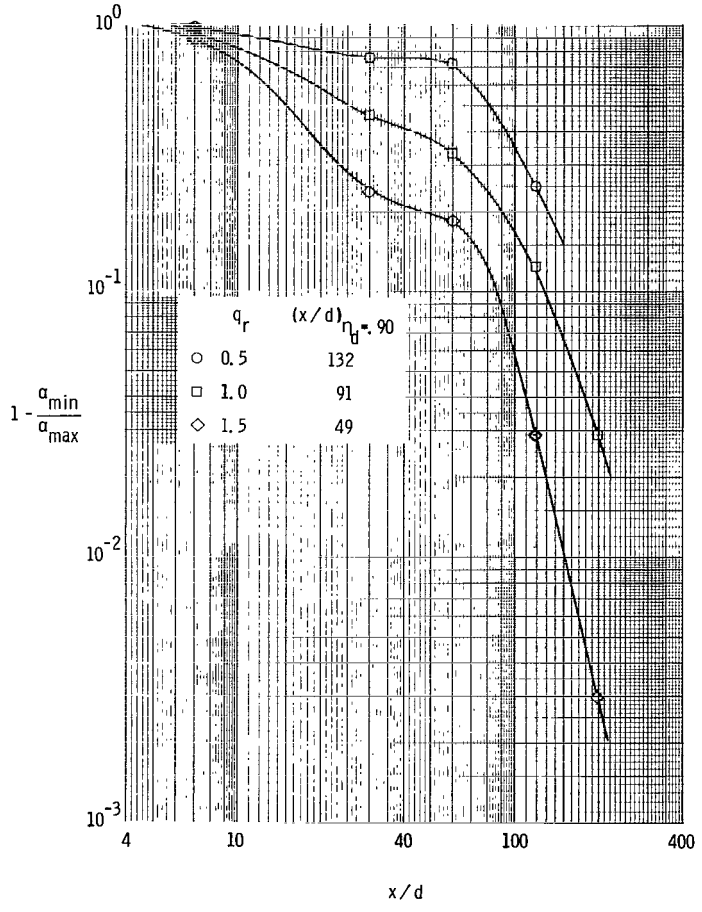

(b) s/d = 6.25.

Figure 8.- Lateral mixing at the point of maximum concentration as measured by the distortion factor.

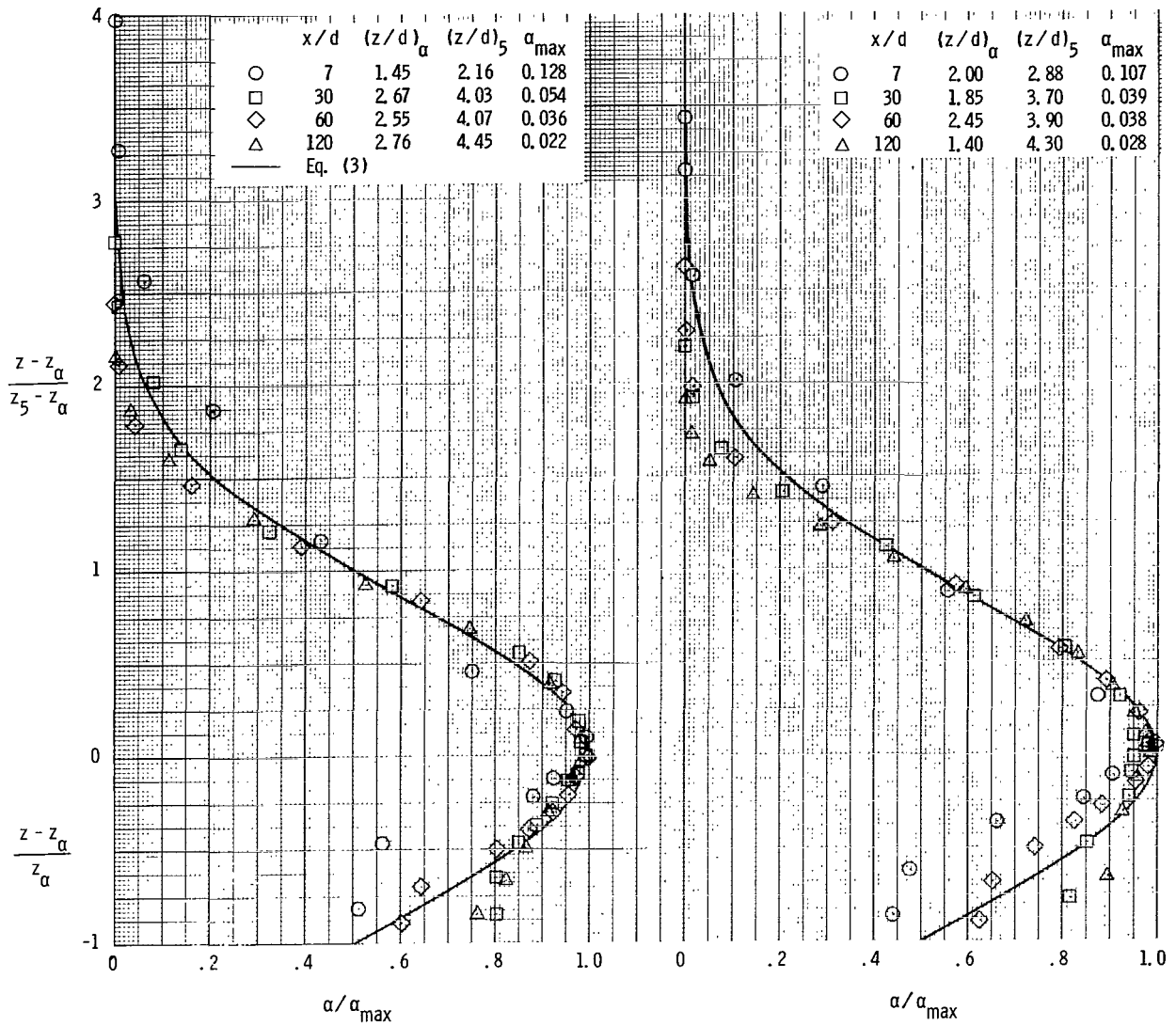

(a) $q_r = 0.5$; $s/d = 12.5$.

(b) $q_r = 0.5$; $s/d = 6.25$.

Figure 9.- Nondimensional concentration profiles compared with Gaussian distribution. Vertical survey.

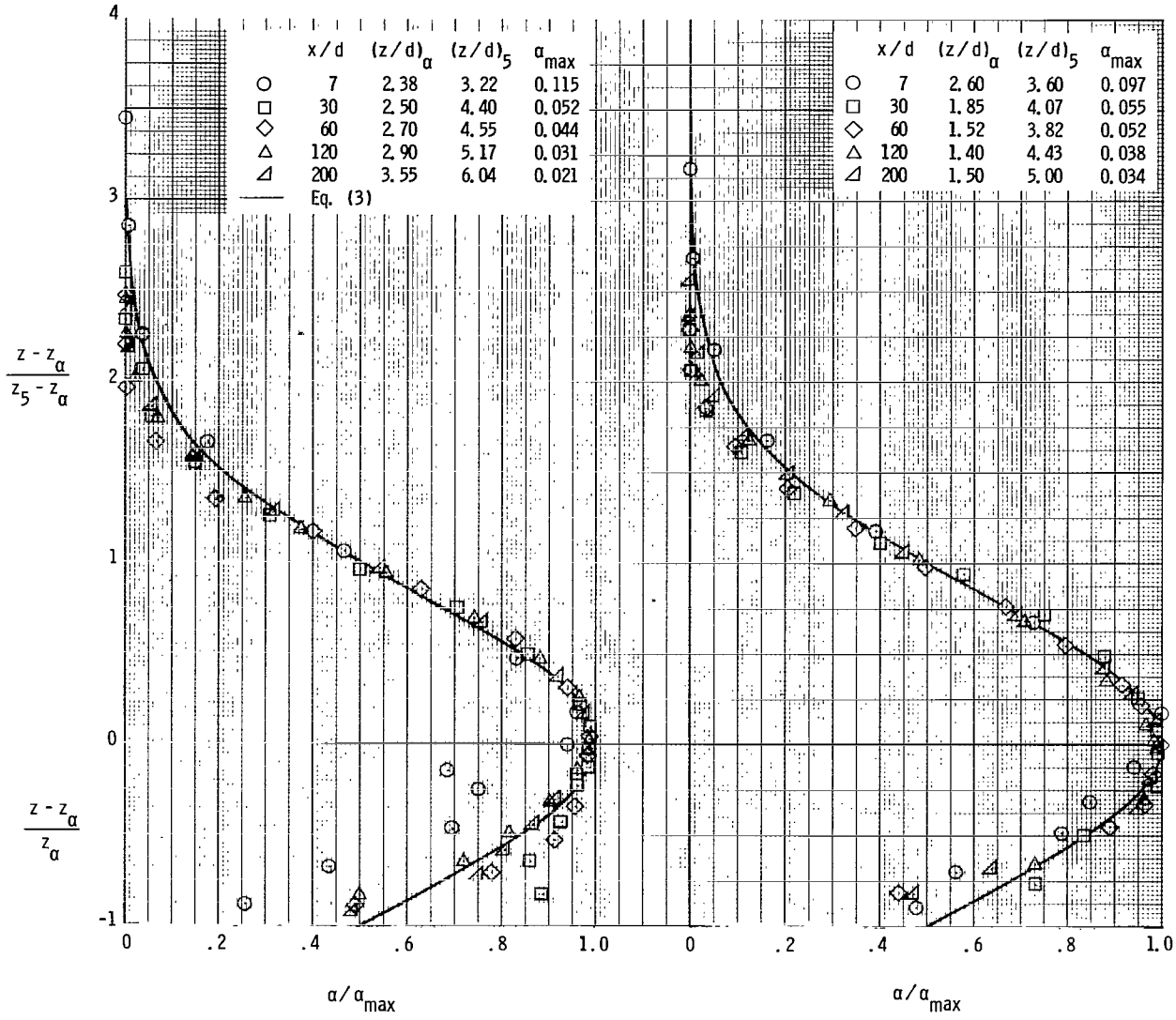

(c) $q_r = 1.0$; $s/d = 12.5$.

(d) $q_r = 1.0$; $s/d = 6.25$.

Figure 9.- Continued.

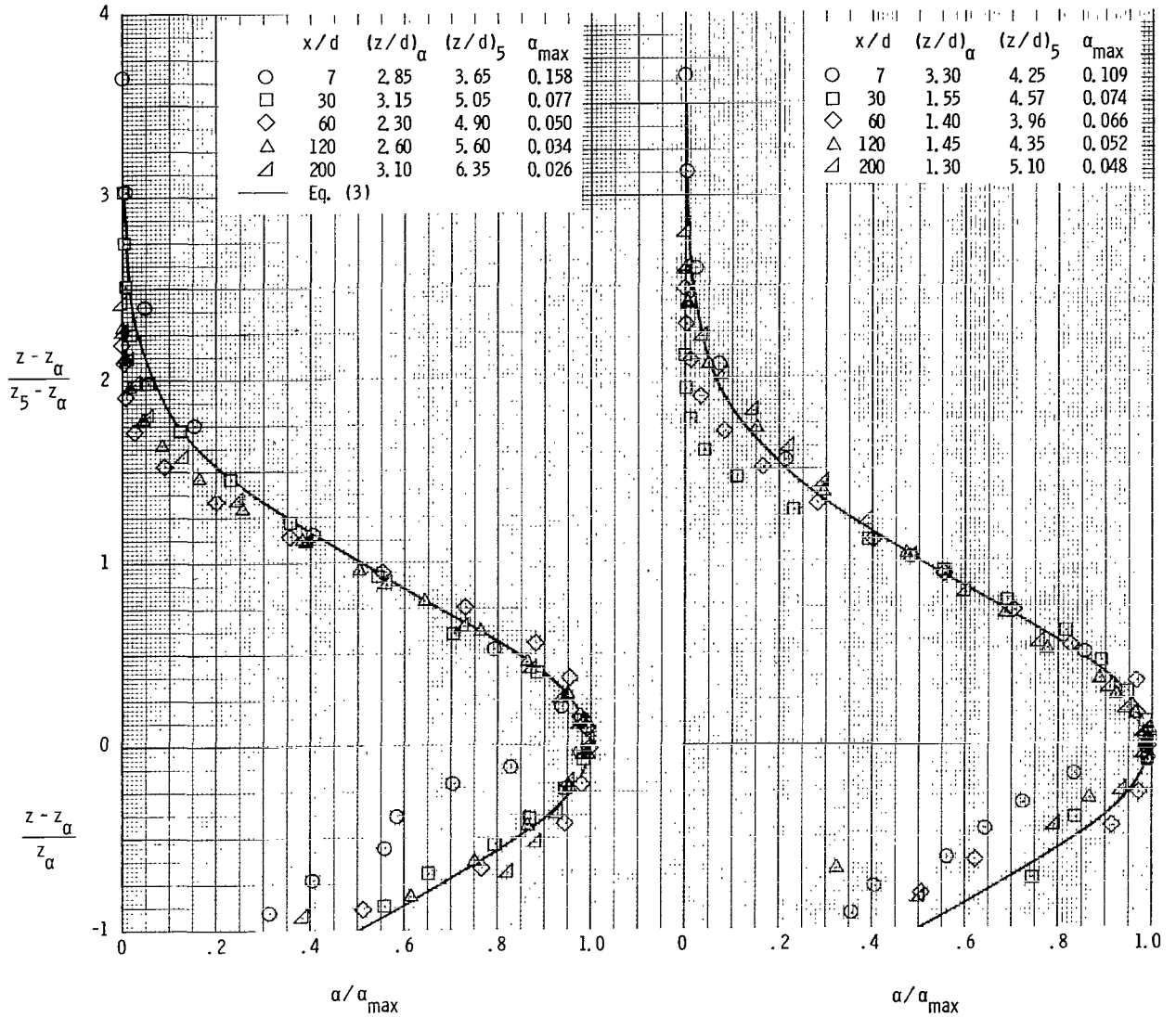

(e) $q_r = 1.5$; $s/d = 12.5$.

(f) $q_r = 1.5$; $s/d = 6.25$.

Figure 9.- Concluded.

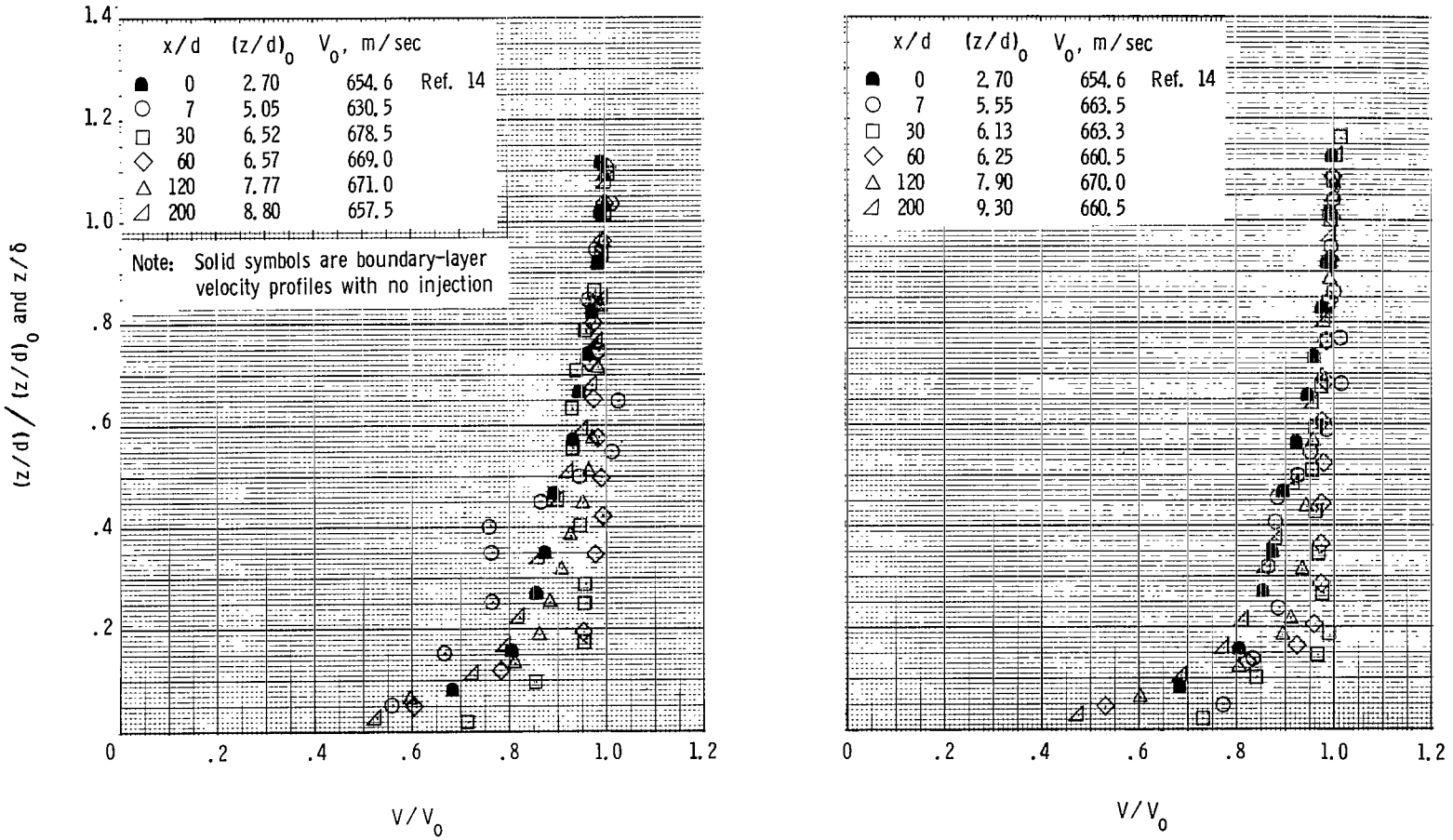

(a) s/d = 12.5.

(b) s/d = 6.25.

Figure 10.- Nondimensional velocity profiles. Vertical survey; $q_r = 1.0$.

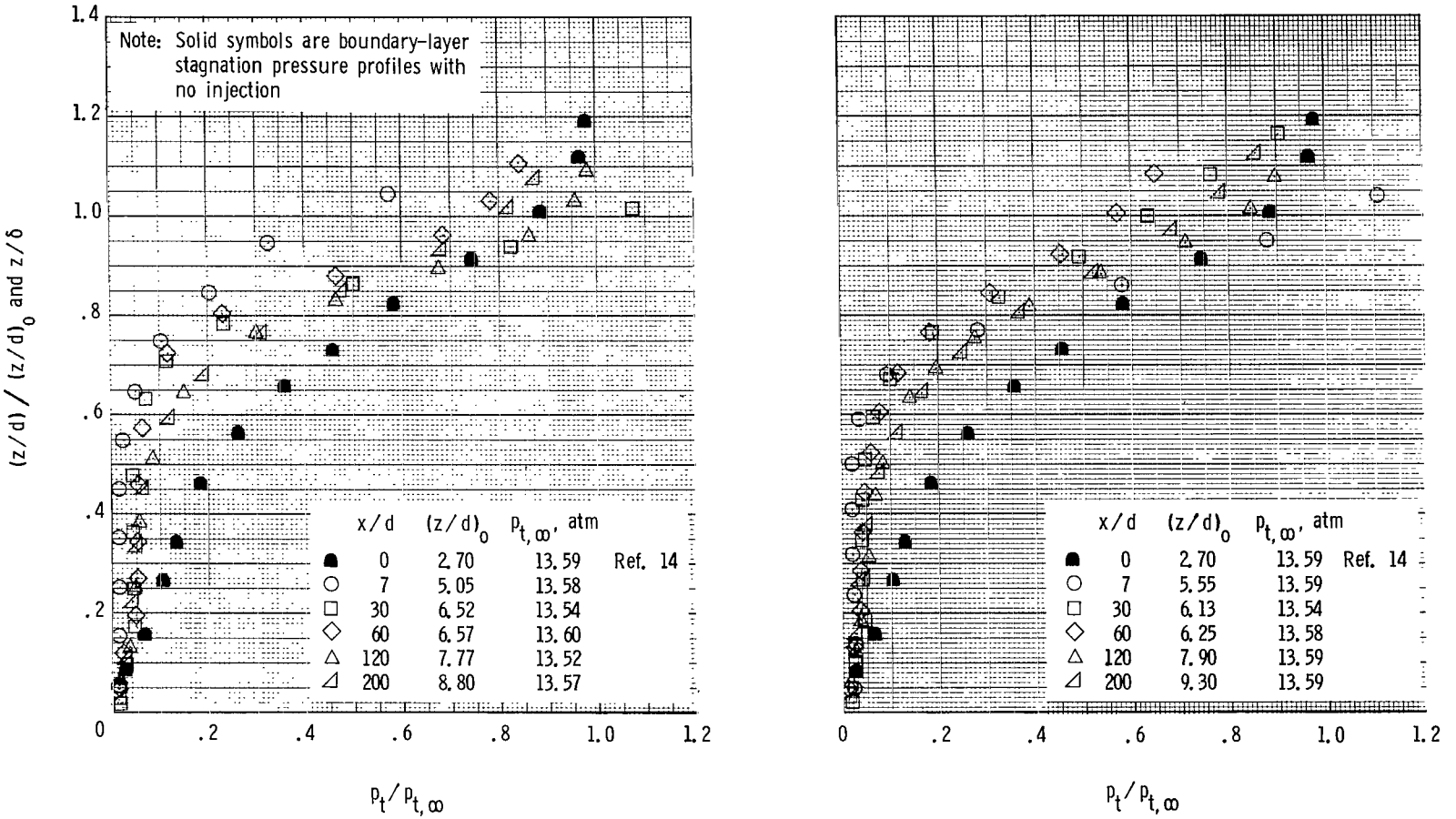

(a) s/d = 12.5.

(b) s/d = 6.25.

Figure 11.- Nondimensional total-pressure profiles. Vertical survey; $q_r = 1.0$.

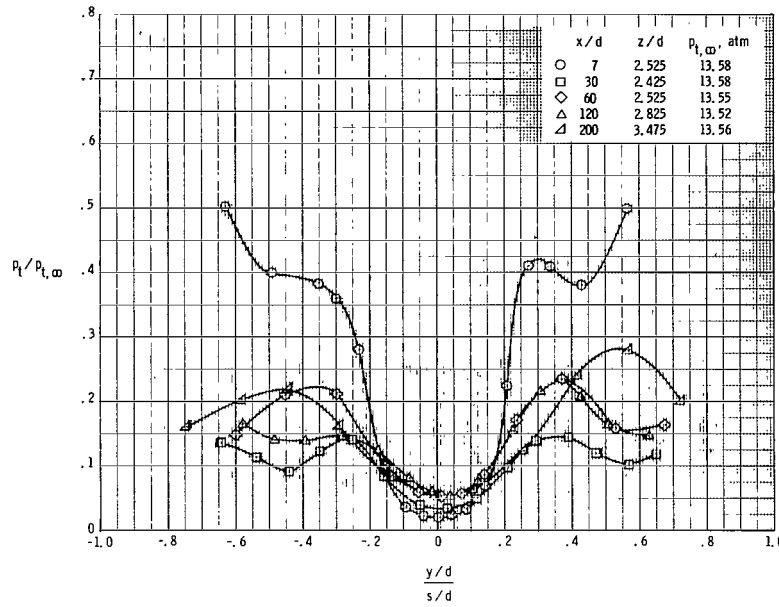

(a) s/d = 12.5.

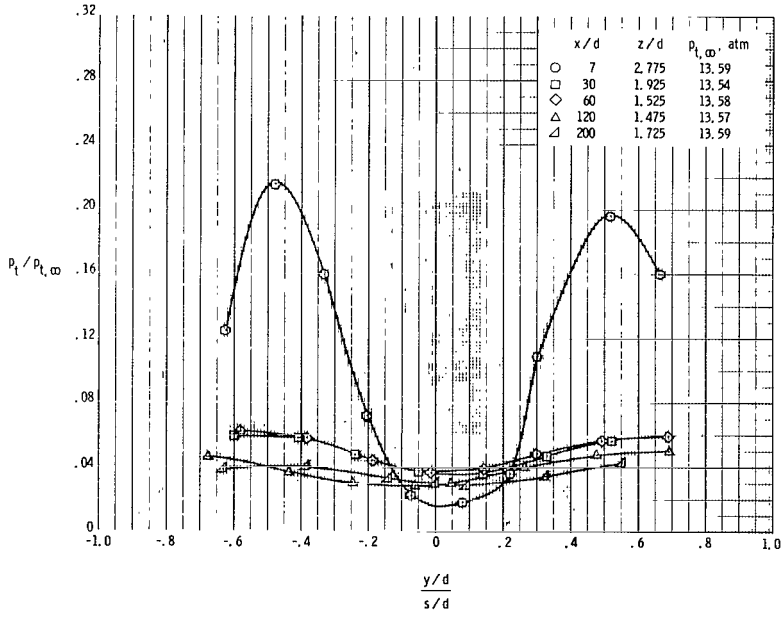

(b) s/d = 6.25.

Figure 12.- Nondimensional total-pressure profiles. Horizontal survey through point of maximum concentration; $q_r = 1.0$.

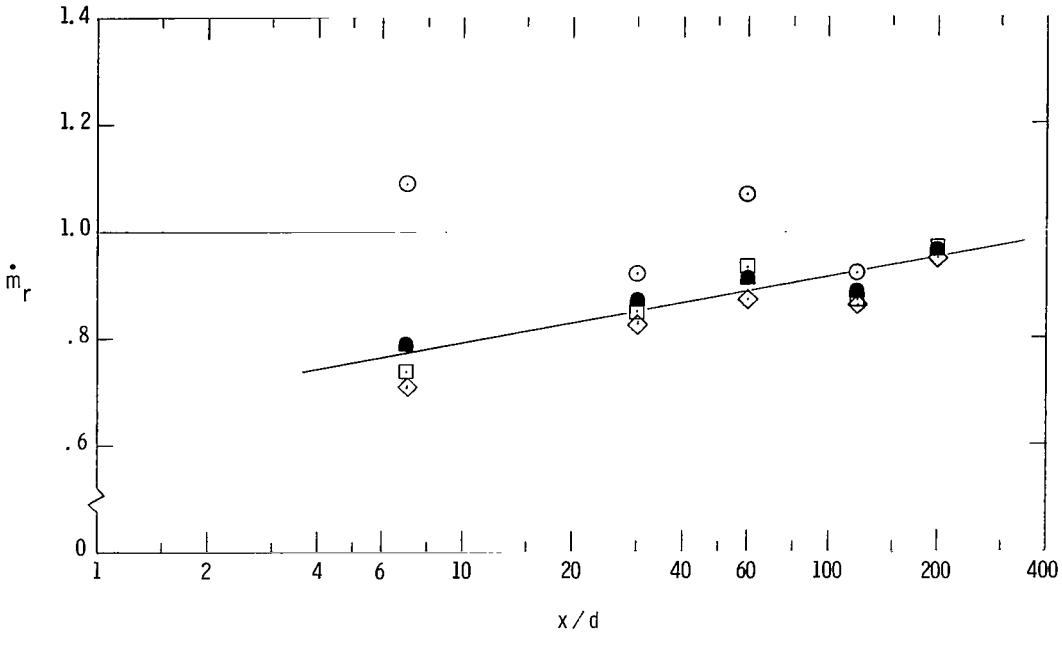

(a) s/d = 12.5.

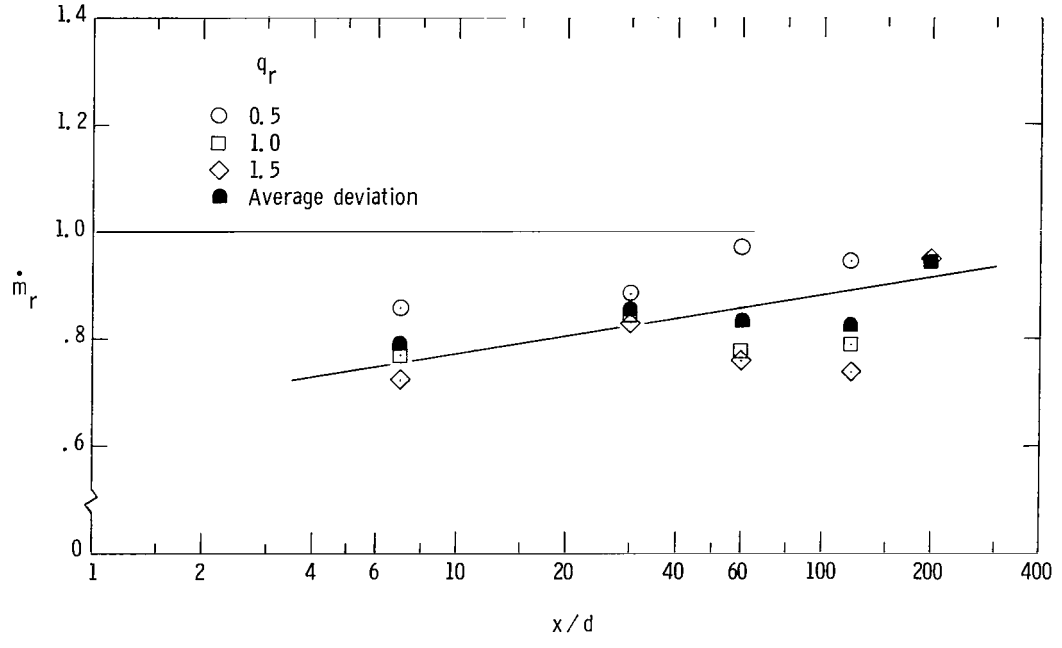

(b) s/d = 6.25.

Figure 13.- Results of integration of hydrogen mass flow rate.

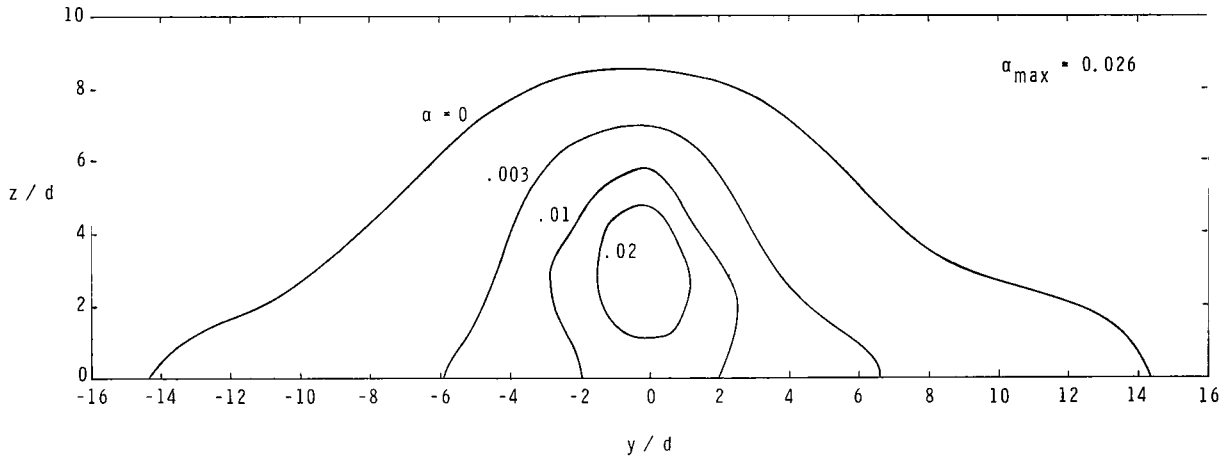

(a) Single jet; $s/d = \infty$.

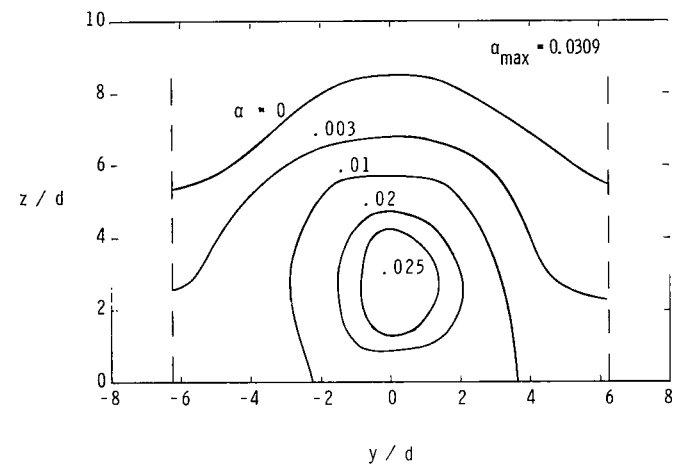

(b) $s/d = 12.5$.

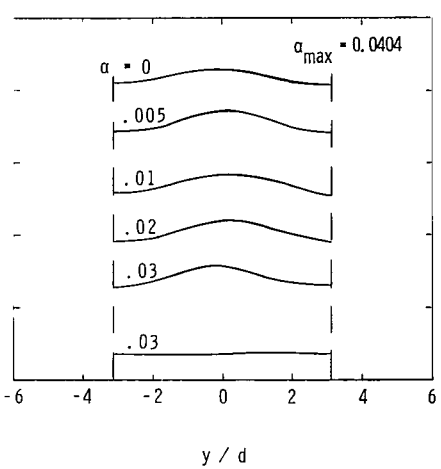

(c) $s/d = 6.25$.

Figure 14.- Typical hydrogen mass concentration contours. $q_r = 1.0$; $x/d = 120$.

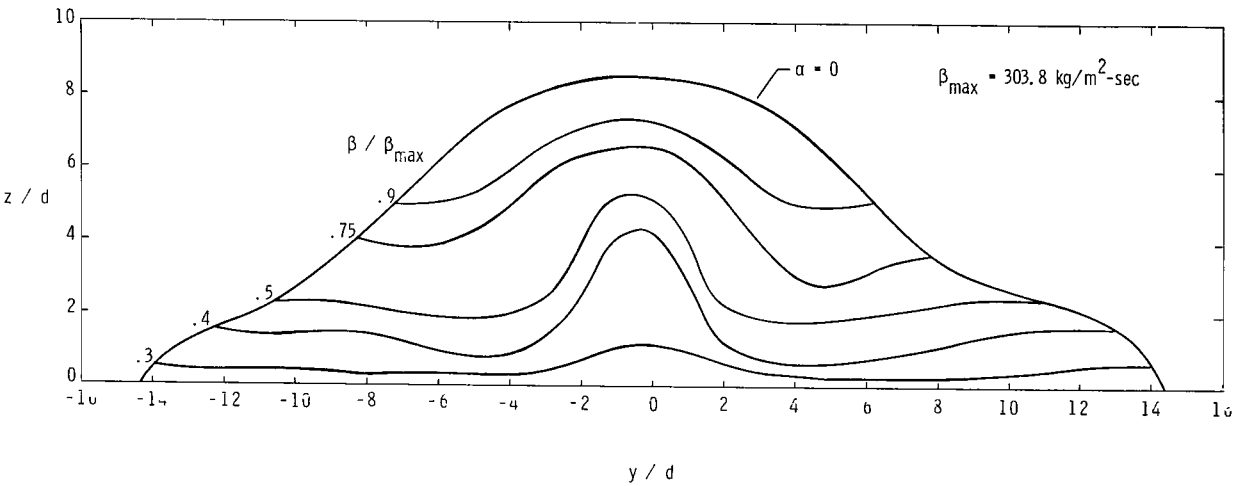

(a) Single injector; s/d = ∞.

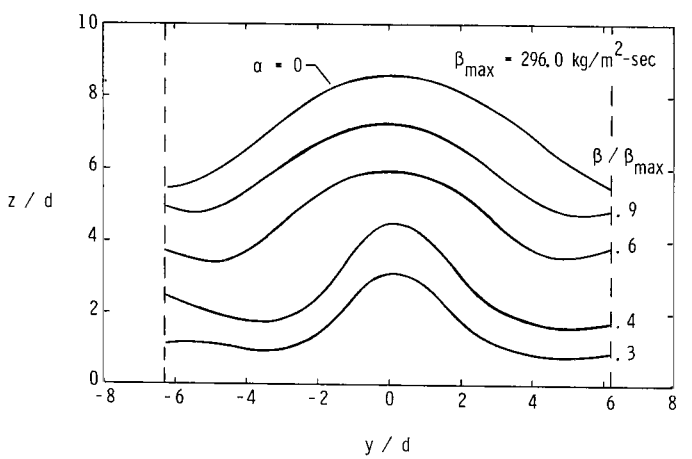

(b) s/d = 12.5.

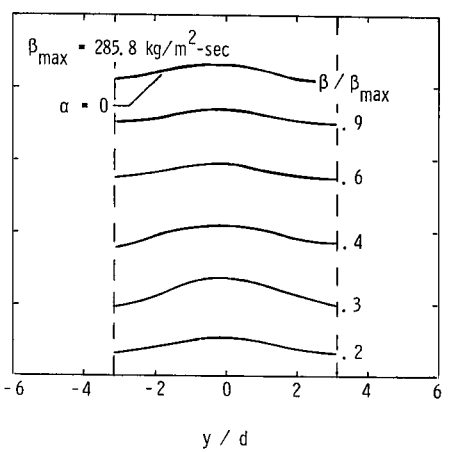

(c) s/d = 6.25.

Figure 15.- Typical air mass flow contours. q_r = 1.0; x/d = 120.

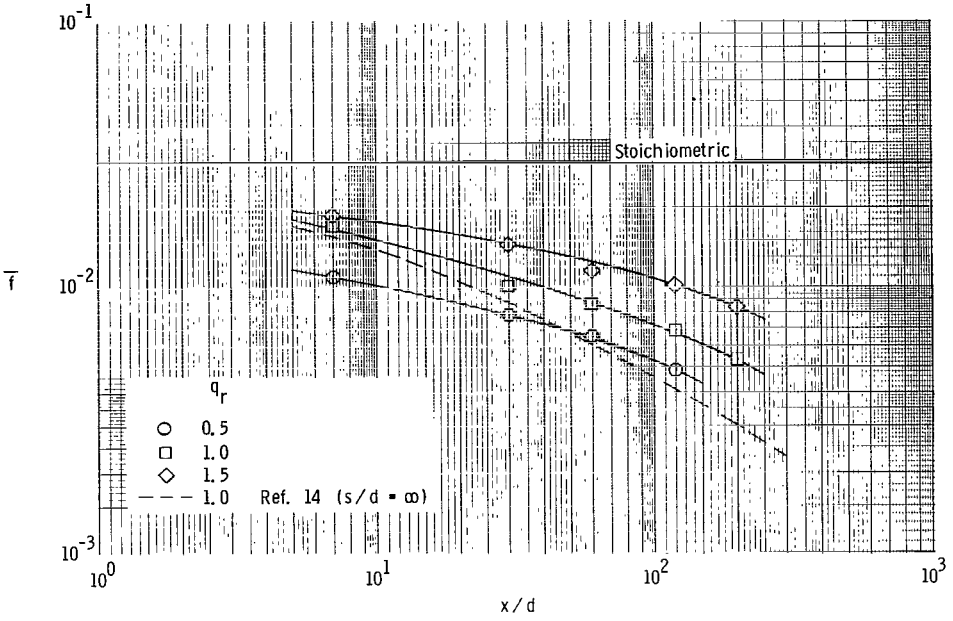

(a) s/d = 12.5.

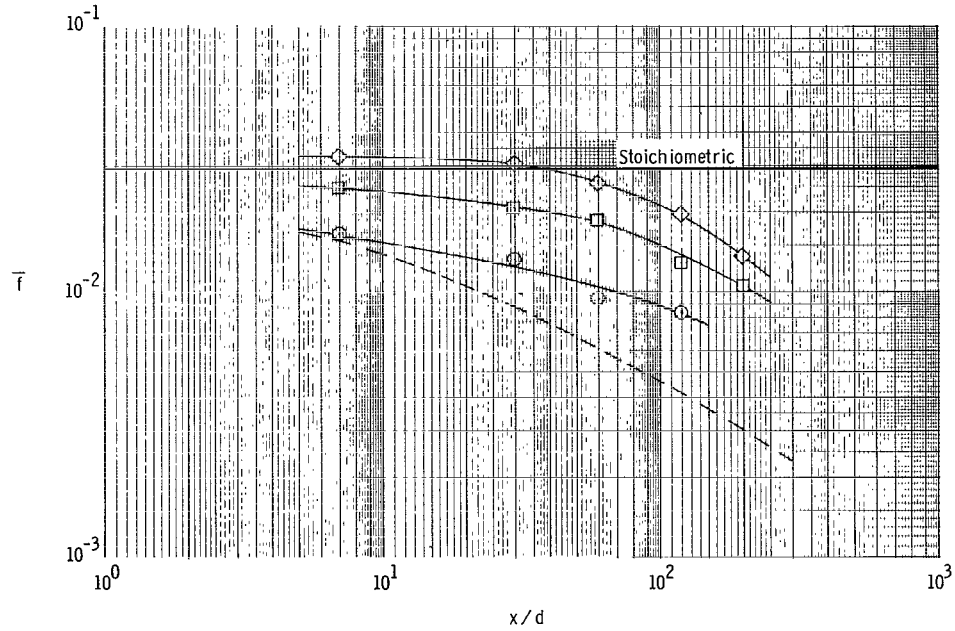

(b) s/d = 6.25.

Figure 16.- Decay of average hydrogen-air mass ratio.

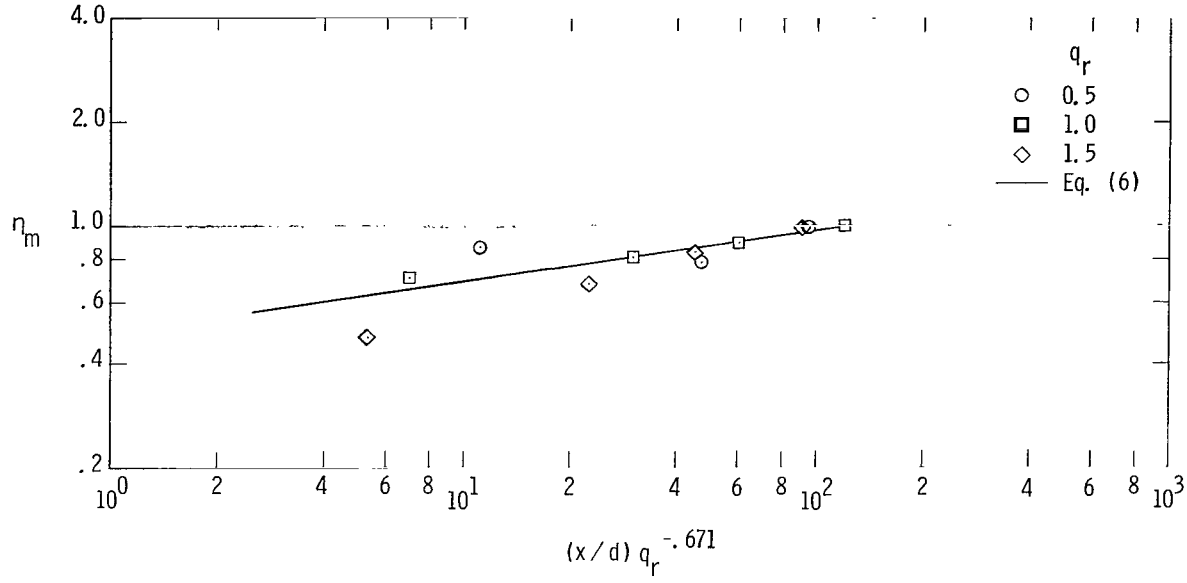

(a) s/d = 12.5.

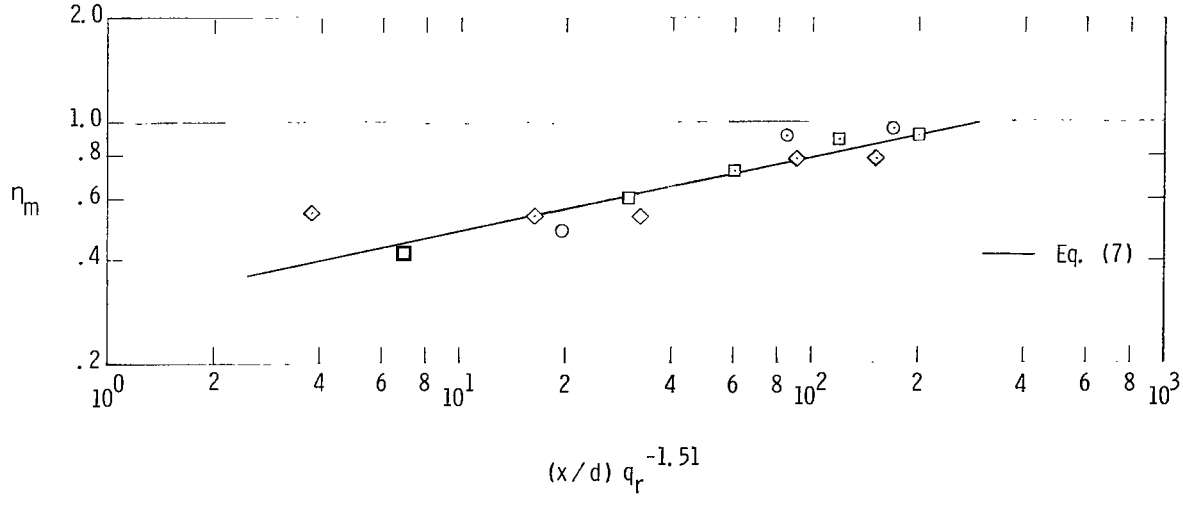

(b) s/d = 6.25.

Figure 17.- Variation of mixing efficiency with downstream distance and dynamic-pressure ratio.

NASA-Langley, 1971 —— 12 L-7896

019 001 C1 U 12 710903 S00903DS
DEPT OF THE AIR FORCE
AF SYSTEMS COMMAND
AF WEAPONS LAB (WLOL)
ATTN: E LOU BOWMAN, CHIEF TECH LIBRARY
KIRTLAND AFB NM 87117

"The aeronautical and space activities of the United States shall be conducted so as to contribute . . . to the expansion of human knowledge of phenomena in the atmosphere and space. The Administration shall provide for the widest practicable and appropriate dissemination of information concerning its activities and the results thereof."

—NATIONAL AERONAUTICS AND SPACE ACT OF 1958

NASA SCIENTIFIC AND TECHNICAL PUBLICATIONS

TECHNICAL REPORTS: Scientific and technical information considered important, complete, and a lasting contribution to existing knowledge.

TECHNICAL NOTES: Information less broad in scope but nevertheless of importance as a contribution to existing knowledge.

TECHNICAL MEMORANDUMS: Information receiving limited distribution because of preliminary data, security classification, or other reasons.

CONTRACTOR REPORTS: Scientific and technical information generated under a NASA contract or grant and considered an important contribution to existing knowledge.

TECHNICAL TRANSLATIONS: Information published in a foreign language considered to merit NASA distribution in English.

SPECIAL PUBLICATIONS: Information derived from or of value to NASA activities. Publications include conference proceedings, monographs, data compilations, handbooks, sourcebooks, and special bibliographies.

TECHNOLOGY UTILIZATION PUBLICATIONS: Information on technology used by NASA that may be of particular interest in commercial and other non-aerospace applications. Publications include Tech Briefs, Technology Utilization Reports and Technology Surveys.

Details on the availability of these publications may be obtained from:

SCIENTIFIC AND TECHNICAL INFORMATION OFFICE

NATIONAL AERONAUTICS AND SPACE ADMINISTRATION

Washington, D.C. 20546